Monthly Notices
of the
ROYAL ASTRONOMICAL SOCIETY

MNRAS **469,** 2662–2671 (2017)
Advance Access publication 2017 April 12

doi:10.1093/mnras/stx904

Spectral performance of SKA Log-periodic Antennas I: mitigating spectral artefacts in SKA1-LOW 21 cm cosmology experiments

Eloy de Lera Acedo,[1⋆] Cathryn M. Trott,[2,3] Randall B. Wayth,[2,3] Nicolas Fagnoni,[1] Gianni Bernardi,[4,5] Brett Wakley,[6] Léon V.E. Koopmans,[7] Andrew J. Faulkner[1] and Jan Geralt bij de Vaate[8]

[1] *Cavendish Laboratory, University of Cambridge, Cambridge, CB3 0HE, UK*
[2] *International Centre for Radio Astronomy Research (ICRAR), Curtin University, Bentley, WA 6102, Australia*
[3] *Australian Research Council Centre of Excellence for All-Sky Astrophysics (CAASTRO), NSW 2006, Australia*
[4] *SKA SA, 3rd Floor, The Park, Park Road, Pinelands, 7405, South Africa*
[5] *Department of Physics and Electronics, Rhodes University, PO Box 94, Grahamstown 6140, South Africa*
[6] *Cambridge Consultants Ltd, Cambridge, CB4 0DW, UK*
[7] *Kapteyn Astronomical Institute, University of Groningen, PO Box 800, NL-9700AV, Groningen, the Netherlands*
[8] *ASTRON, the Netherlands Institute for Radio Astronomy, Postbus 2, NL-7990 AA Dwingeloo, the Netherlands*

Accepted 2017 April 10. Received 2017 April 4; in original form 2017 February 16

ABSTRACT

This paper is the first in a series of papers describing the impact of antenna instrumental artefacts on the 21 cm cosmology experiments to be carried out by the low frequency instrument (SKA1-LOW) of the Square Kilometre Array telescope (SKA), i.e. the Cosmic Dawn (CD) and the Epoch of Reionization (EoR). The smoothness of the passband response of the current log-periodic antenna being developed for the SKA1-LOW is analysed using numerical electromagnetic simulations. The amplitude variations over the frequency range are characterized using low-order polynomials defined locally, in order to study the impact of the passband smoothness in the instrument calibration and CD/EoR Science. A solution is offered to correct a fast ripple found at 60 MHz during a test campaign at the SKA site at the Murchison Radio-astronomy Observatory, Western Australia in 2015 September with a minor impact on the telescope's performance and design. A comparison with the Hydrogen Epoch of Reionization Array antenna is also shown demonstrating the potential use of the SKA1-LOW antenna for the delay-spectrum technique to detect the EoR.

Key words: instrumentation: detectors – dark ages, reionization, first stars.

1 INTRODUCTION

The Square Kilometre Array (SKA)[1] is a next generation radio telescope, with unprecedented sensitivity and survey speed. The SKA will explore the Southern hemisphere skies faster and deeper than any other radio telescope has ever done. Spread across two continents (Southern Africa and Australia + New Zealand), it will cover a frequency range from 50 MHz up to 14 GHz and will tackle fundamental problems in modern Astrophysics including the study of the cosmic dawn (CD) and the Epoch-of-Reionization (EoR) as described in Koopmans et al. (2015). Phase I of the SKA will have a lower frequency instrument (SKA1-LOW: 50–350 MHz) that will be used for the study of the early epochs of the Universe by looking at the redshifted signal from the 21 cm Hydrogen emission line. This instrument will be located in Western Australia. It will be a 512 station interferometer with baselines up to 60 km and more than 130 000 antenna elements (Turner 2015). Each station has been designed as a pseudo-random array of wide band antennas in order to minimize the effects of mutual coupling as shown by Gonzalez-Ovejero et al. (2011) and de Lera Acedo et al. (2011) and the effects of side-lobes (Razavi-Ghods et al. 2012; El-makadema, Rashid & K. Brown 2014). Each station is 35 m in diameter in order to meet the desired beam-width (Mellema et al. 2013; Koopmans et al. 2015).

The SKA1-LOW antenna is proposed to be a log-periodic dipole array, SKA Log-periodic Antenna (SKALA). Version 1 of SKALA, SKALA-1 was described in de Lera Acedo et al. (2015b). SKALA-1 maximizes the telescope's sensitivity over the field of view across the 7:1 frequency band due to its moderate-to-high directivity and flat impedance, in contrast to dipole antennas that have low-directivity values and only show relatively flat impedance over a narrow frequency band (typically 2:1 or 3:1 at most).

⋆ E-mail: eloy@mrao.cam.ac.uk
[1] http://www.skatelescope.org

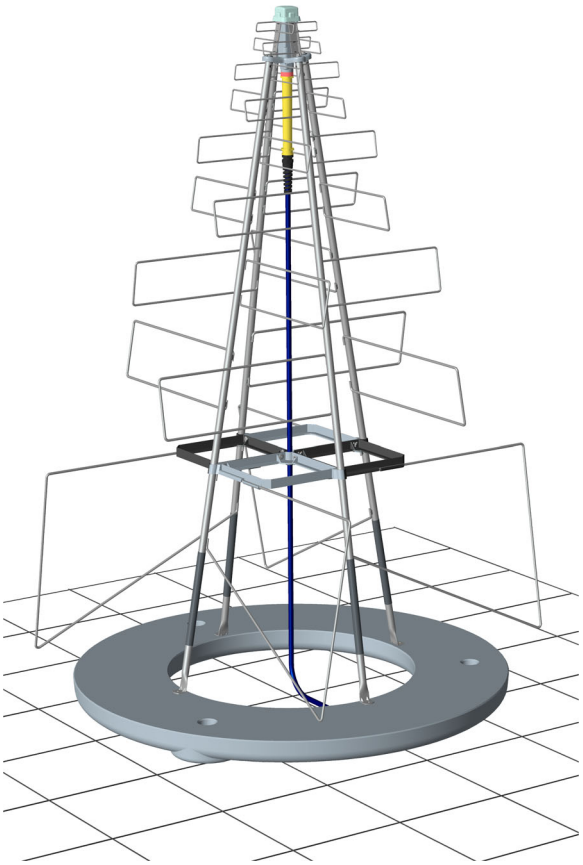

Figure 1. Computer model of SKALA-2 antenna on top of a metallic ground plane (the ground plane is a mesh of wires with 30 cm pitch). The antenna is a log-periodic dipole array made of four identical metallic arms forming two polarizations with nine dipoles each. The grey ring is the base of the antenna. The cabling coming down vertically in the centre of the antenna is the optical fibre and power cable. The top enclosure with a green cap hosts the low-noise amplifiers and an RF-over-Fibre transmitter. The antenna has a footprint of 1.2 × 1.2 m and a height of 1.8 m.

Subsequently, a mechanical upgrade of SKALA-1 was designed and built, SKALA-2, in order to improve the design for mass manufacturing with negligible impact on the electromagnetic performance of the antenna. This upgraded design was presented in de Lera Acedo et al. (2015a). A computer model of the SKALA-2 antenna is shown in Fig. 1. This paper describes the modifications to the length of the SKALA-2 antenna arms and component values of capacitors and inductors in the input matching network of the low-noise amplifier (LNA) in order to improve the spectral smoothness of the antenna system. The result of this improvement is SKALA-3.

Both the CD and EoR observations require a smooth response of the instrument across frequency to enable the detection of the faint signals buried in much brighter foreground signals and not to introduce instrumental spectral structure on scales of relevance for the neutral hydrogen signal (Parsons et al. 2012; Trott & Wayth 2016; DeBoer et al. 2017).

This paper describes the analysis of the proposed SKA1-LOW antenna, SKALA-3, using a local low-order polynomial fitting in order to assess its performance against realistic CD/EoR science requirements. In Section 2, the requirements derived in Trott & Wayth (2016) are summarized. Section 3 describes the current antenna topology and performance. Section 4 focuses on the description of the analysis and the results from numerical simulations.

Table 1. Requirements from Trott & Wayth (2016). δ is the normalized fractional residual after a third-order polynomial fitting.

Frequency (MHz)	δ
50	0.025
100	0.01
150	0.005
200	0.008

Section 5 presents the improved bandpass smoothness to meet the science requirements of the proposed SKA1-LOW antenna. Section 6 shows a comparison with the Hydrogen Epoch of Reionization Array (HERA[2]) antenna against requirements derived for the delay-spectrum technique for EoR observations. Finally, Section 7 draws some conclusions.

2 SPECTRAL CALIBRATION REQUIREMENTS

In Trott & Wayth (2016) a formal procedure for the derivation of spectral requirements for radio interferometers dedicated to 21 cm cosmology experiments is presented. Here, we use the requirements derived in that paper to assess the design of the SKALA-2 and SKALA-3 antennas. In a companion paper (Trott et al. 2017, Paper II), we use realistic simulations to test the calibration performance of these antennas and a comparison dipole (Tingay et al. 2013; Wayth et al. in preparation, the Murchison Widefield Array - Engineering Development Array).

One of the spectral requirements affects the EoR Power spectrum pipeline and is related to the level of the amplitude residuals after fitting a low-order polynomial locally to the station's complex-valued voltage gain passband. The power derived from fitting a low-order ($n = 2, 3, 4$) polynomial over three contiguous coarse channels (2.25 MHz) yields structured power in the power spectrum space. This power is less than the thermal noise, but has the potential to cause low-level bias in the derived science results due to its shape. Table 1 lists the relative fractional bandpass errors tolerable in a fourth-order polynomial residual on voltage gain amplitudes at four different frequencies (In Trott & Wayth 2016, requirements were also derived for second- and fourth-order polynomial fittings). Strictly speaking, this should be applied to the station beam passband. Our current analysis has been done at the antenna level, which will dominate the passband response of the instrument. Further analysis is needed to include station beam effects such as mutual coupling and other antenna effects such as polarization and the instrument's response across the whole field of view (including spectral variations in the far field pattern of the antenna).

Furthermore, in Trott & Wayth (2016) requirements are derived for the necessary smoothness in the phase passband of the station's voltage gain. Phase residuals affect the imaging (tomography) experiment substantially. The so-called 'phase noise' decorrelates the visibilities and adds an effective noise to the images that swamps the signal. So, in Trott & Wayth (2016) the maximum change in phase across any fine channel (within the 100–200 MHz band) that would lead to the swamping of the expected EoR signal is computed. In the worst case where the phase residual on each channel is fixed over the full experiment, there cannot be more than a 0.04 deg. change of phase over any fine channel (4.58 kHz). An optimistic case where

[2] http://reionization.org

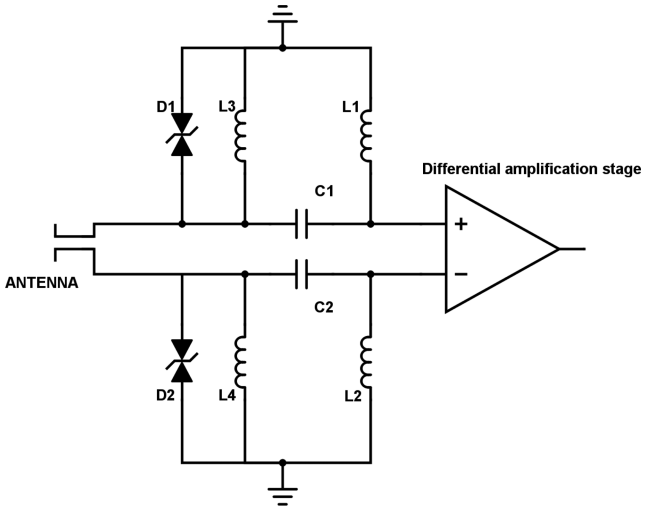

Figure 2. Simplified RF schematic model of the first amplification stage of the LNA. The S-parameters and noise parameters for the transistors used in this design are obtained from the manufacturers. This diagram highlights the key components in the input side of the LNA that have been used for the improvement of the design (the DC blocking capacitors C1 and C2, the bias inductors L1 and L2 and the ESD shunt inductors L3 and L4). The ESD diodes D1 and D2 are also shown here. For the simulations in this paper the full model of the LNA also included the second stage transistor, although this has a small effect on the matching with the antenna.

the phase residual is uncorrelated in time between calibration cycles, yielding an increase in dynamic range and weaker constraints, raises that limit to 0.2 deg.

3 SKALA ANTENNA AND LNA PERFORMANCE

The SKALA-1 and SKALA-2 antennas were designed to maximize the sensitivity of the SKA1-LOW instrument across at least a 7:1 frequency band by means of optimizing its effective area, minimizing its footprint and average distance between elements (to maximize brightness sensitivity for a fixed number of elements) and reducing receiver noise (dominated by the matching between the antenna and the first stage low-noise amplifier).

The antenna simulations were carried out using Computer Simulation Technology (CST)[3] for the antenna and Microwave Office[4] for the LNA. The LNA design is based on a pseudo-differential configuration with a first differential amplification stage using Qorvo[5] transistors (TQP3M9039) and a second amplification stage after a wide band balun transformer using a Mini-Circuits[6] transistor (PSA-5451+). Fig. 2 shows the simplified schematic of the first amplification stage. Fig. 3 shows the input LNA impedance ($Z_{\rm LNA}$), the LNA optimum noise impedance at the centre of the noise circles ($Z_{\rm opt}$) and the antenna input impedance ($Z_{\rm A}$) across frequency. It is well known that the process of noise matching and power matching calls for a trade-off between achieving a low noise figure and a smooth passband with maximum power transfer (Pozar 2011). Fig. 3 shows that the optimum noise impedance of the LNA to which we need to match our antenna for minimum noise figure; and the input impedance of the LNA to which we need to match our antenna impedance for maximum power transfer, are not in the same place in the Smith chart. SKALA-1 was originally designed to cover the band of 70–450 MHz and it was later optimized to work down to 50 MHz with the focus on maximum sensitivity and therefore minimum receiver noise, hence it is matched to the optimum noise impedance of the LNA. The noise figure of the LNA connected to SKALA-2 is shown in Fig. 4 and the passband is shown in red in Fig. 8 and Fig. 9. The *passband* here is the voltage gain of the LNA, $G_{\rm LNA}$, when connected to the antenna impedance (not a fixed reference impedance), thus the performance is as it would be in a real scenario. The antenna was simulated standing on top of an infinite perfect electric conductor ground plane. A low-receiver noise was achieved down to 100 MHz where the sky noise starts to severely dominate the system noise and we can relax the receiver noise requirements. However, the passband response of the LNA when connected to the antenna impedance, exhibits several sharp features, especially one around 60 MHz.

It is important to notice that according to the definition of sensitivity used here and described by equation (1) (effective area over system temperature or signal over noise) the passband smoothness will not be visible in that metric. The reason for this is that the ratio of effective area over system noise temperature is constant independent of where the ratio is taken in the receiving chain. In equation (1) we refer this ratio to the input of the LNA and therefore both effective aperture and system noise temperature (all of the noise terms) will be equally weighted by the gain of the LNA, as if we try to calculate this ratio at the output of the LNA. This is correct as long as we have taken into account the noise contribution from the rest of the receiving chain (after the LNA) weighted by the gain of the previous stages (in order to refer it to the input of the LNA). Since the gain of the LNA is high and the noise figure of the following stages is small, this contribution is negligible. Consequently, the effect of the passband gain of the LNA will not be visible in the sensitivity values. In equation (1), λ is the wavelength, $D_{\theta,\psi}$ is the antenna's directive gain, η is the radiation efficiency, $T_{\rm A}$ is the antenna temperature (including the sky temperature), T_0 is the ambient temperature (295 K) and $T_{\rm rec}$ is the receiver noise temperature. For more details, see de Lera Acedo et al. (2015b).

$$\left(\frac{A_{\rm eff}}{T_{\rm sys}}\right)_{\theta,\psi} = \frac{\frac{\lambda^2}{4\pi} D_{\theta,\psi}\eta}{\eta T_{\rm A} + (1-\eta)T_0 + T_{\rm rec}} \quad (1)$$

4 SPECTRAL ANALYSIS USING LOCAL LOW-ORDER POLYNOMIAL FITTING

In this section, we analyse the response of the SKALA-2 antenna measuring it against the requirements presented in Trott & Wayth (2016). As mentioned before, we simulate the passband of one antenna alone because it dominates the passband response across frequency of the station beam. Furthermore, we focus on the passband response of the LNA when connected to the antenna omitting the effect of the antenna far field pattern since this is much more smooth than that of the LNA and will not affect these results. The frequency band (50–350 MHz) is subdivided into coarse channels 750 kHz wide, each of which is subdivided into fine channels 4.6 kHz wide. This means 163 fine channels per every coarse channel. We fit an nth-order polynomial (by default in this paper the order is three) to all fine frequency channels in a least-squares sense across m coarse channels (by default in this paper m is three as well) to both

[3] Computer Simulation Technology AG, http://www.cst.com
[4] http://www.awrcorp.com/products/ni-awr-design-environment/microwave-office
[5] http://www.qorvo.com
[6] http://www.minicircuits.com

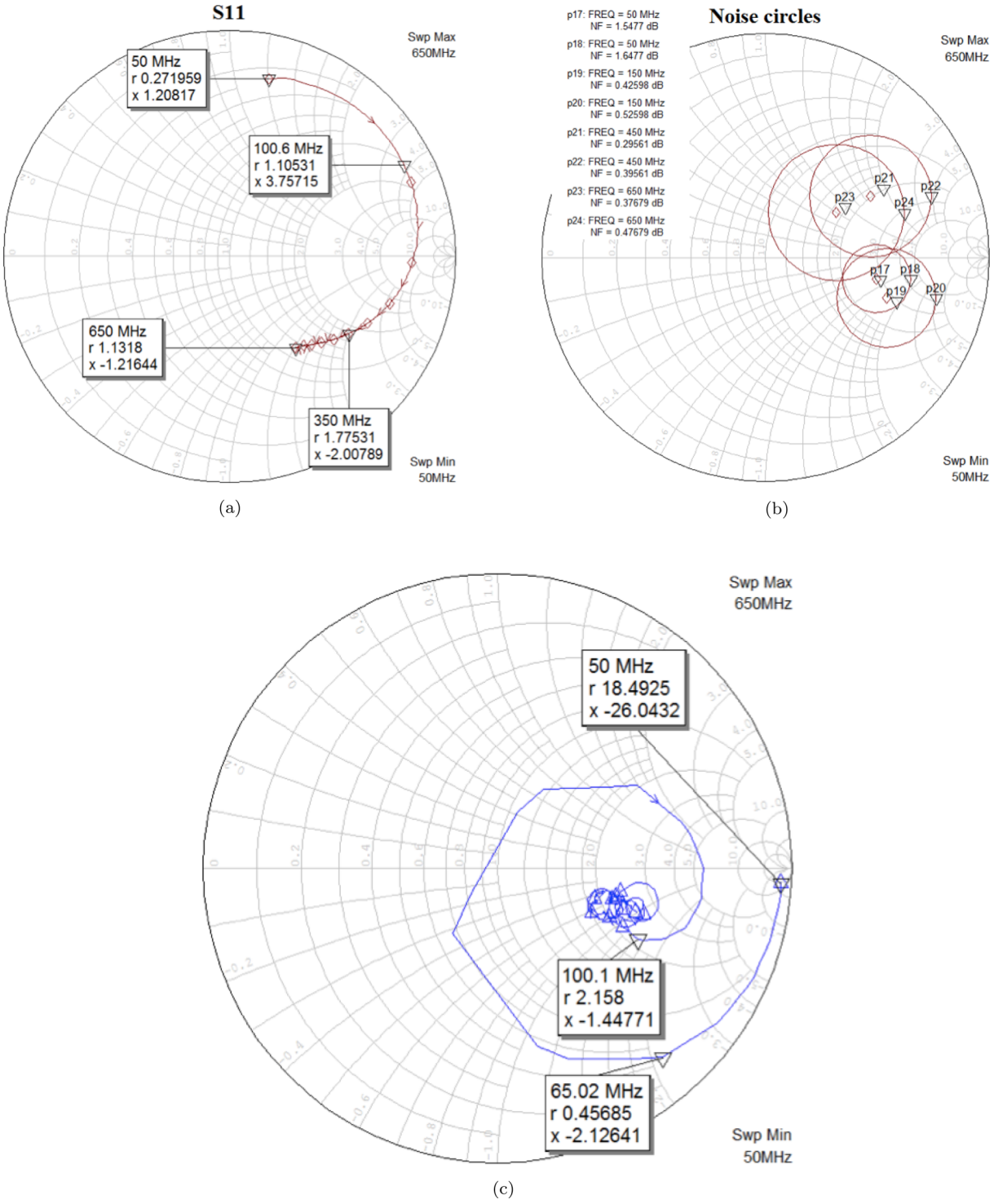

Figure 3. Antenna and LNA impedances; (a) LNA input impedance for power match, (b) LNA noise circles for noise match and (c) Antenna input impedance. The Smith chart is plotted on the complex reflection coefficient plane in two dimensions. The horizontal axis corresponds to a purely real reflection coefficient and the centre is the reference impedance, 50 Ω.

the real and imaginary parts of the passband. The fitted complex passband (S^*), where the fit has been performed separately to its real part (S_r^*) and its imaginary part (S_i^*), follows the definition of equation (2) (ν is the frequency and ν_0 is the central frequency for each coarse channel). The polynomial fit is only used to model the fine channels corresponding to the middle coarse channel of the m channels used to generate the fit. We can then subtract the model of the amplitude response from the amplitude of the passband data (S) and normalize this difference by S again to get the residuals (δ) as in equation (3). This process is repeated for all the fine channels in the frequency bandwidth by moving the central coarse channel by one (and consequently fitting the next set of fine channels) to obtain the wide-band performance of the antenna. While the default bandwidth used for the polynomial fitting in this paper is 2.25 MHz

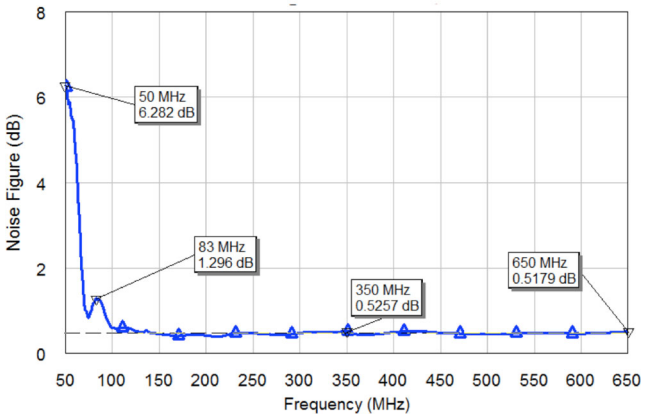

Figure 4. Noise figure of LNA when connected to SKALA-2.

(three coarse channels), in Barry et al. (2016) it is recommended that smoothness is also achieved in larger bandwidths in order to prevent contamination of the relevant modes for the EoR detection. We have therefore extend our analysis here to nine coarse channels (6.75 MHz). The choice of the order of the polynomial is also important, since high orders could constrain the fit in excess and remove not only the instrument's passband, but also the cosmological signal. Furthermore, high-order polynomial fittings would result as well in high-order residuals at potentially similar spectral scales to that of the cosmological signal. While we have stayed at a relatively low order here (equation 3), in Trott et al. (2017) the effects of using higher order polynomials are also discussed.

$$S^*_{r,i}(\nu) = A(\nu - \nu_0)^3 + B(\nu - \nu_0)^2 + C(\nu - \nu_0)^1 + D \tag{2}$$

$$\delta(\nu) = \frac{||S^*(\nu)| - |S(\nu)||}{|S(\nu)|} \tag{3}$$

The phase gradient per fine channel, $\Delta(\nu)$, is calculated using equation (4).

$$\Delta(\nu) = \frac{\mathrm{d}\big/S(\nu)}{\mathrm{d}\nu} * 4.6\,\mathrm{kHz} \tag{4}$$

Fig. 5 shows how the required residuals are not met by SKALA-2 at the frequency where the passband has peaked behaviour in amplitude and a fast slope in the phase due to the mismatch between the antenna and the LNA. The phase gradient requirement seems to be more under control than the amplitude requirement, especially in the band 100–200 MHz, although it is again higher at lower frequencies as indicated in Fig. 6.

5 IMPROVEMENT OF THE BANDPASS SMOOTHNESS

5.1 Antenna and LNA modifications

The spectral response of the antenna is dominated by the mismatch between the antenna and the first stage low-noise amplifier. In order to improve the power match between the antenna and the low-noise amplifier, we have explored modifications of both systems specifically where we were not meeting the passband requirements (50–100 MHz).

In SKALA-3, we have modified the input network of the LNA (see Fig. 2) using the original input matching components but with a lower value of the Direct Current (DC) blocking capacitors and bias inductors [150 nH Electrostatic discharge (ESD) shunt inductors remain the same (L3 and L4), 24 pF DC blocking capacitors (C1 and C2) 270 nH bias inductors (L1 and L2)]. The trade-off is a higher noise figure, peaking at almost 8.6 dB at 57 MHz. This is a side effect of using a smaller value inductor in the bias network after we added a resistor for stability. We don't want to change that resistor, and making that inductor larger immediately sharpens the peak in the gain response. The series capacitor could be reduced in value to smooth the ripple even further, but the peaking in the noise

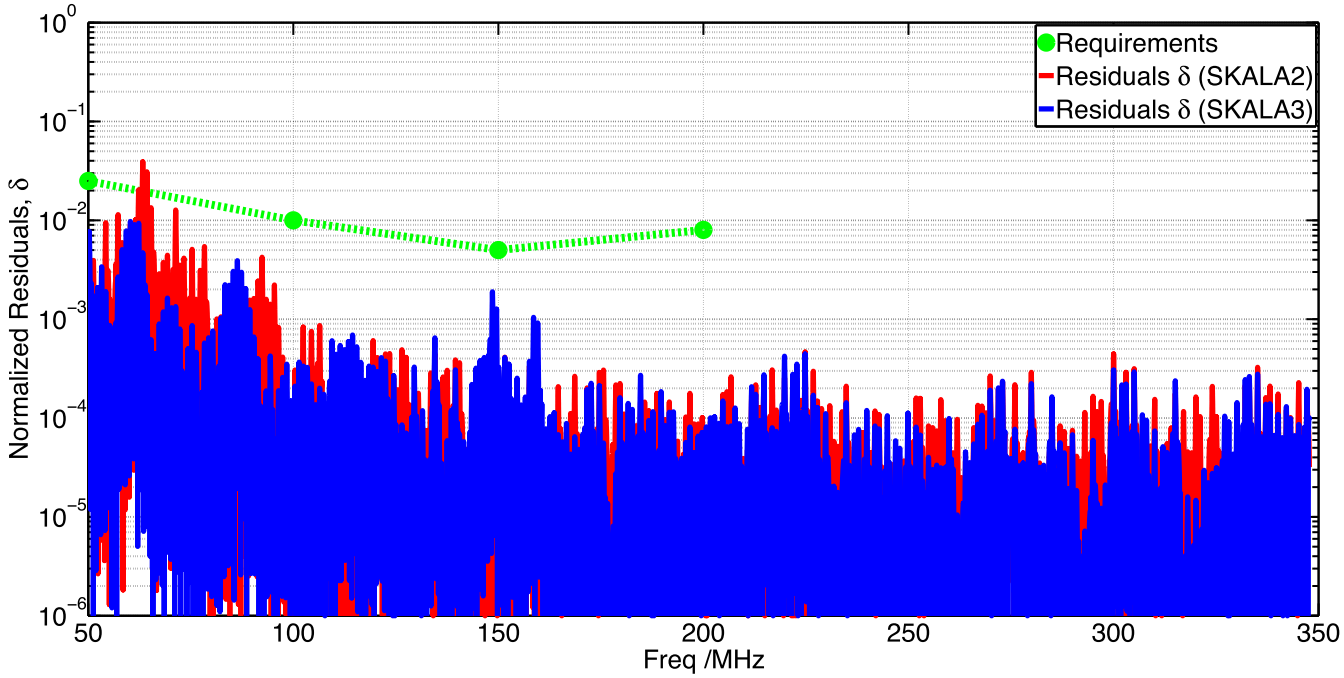

Figure 5. Residuals after a third-order local polynomial fitting using SKALA-2 and SKALA-3.

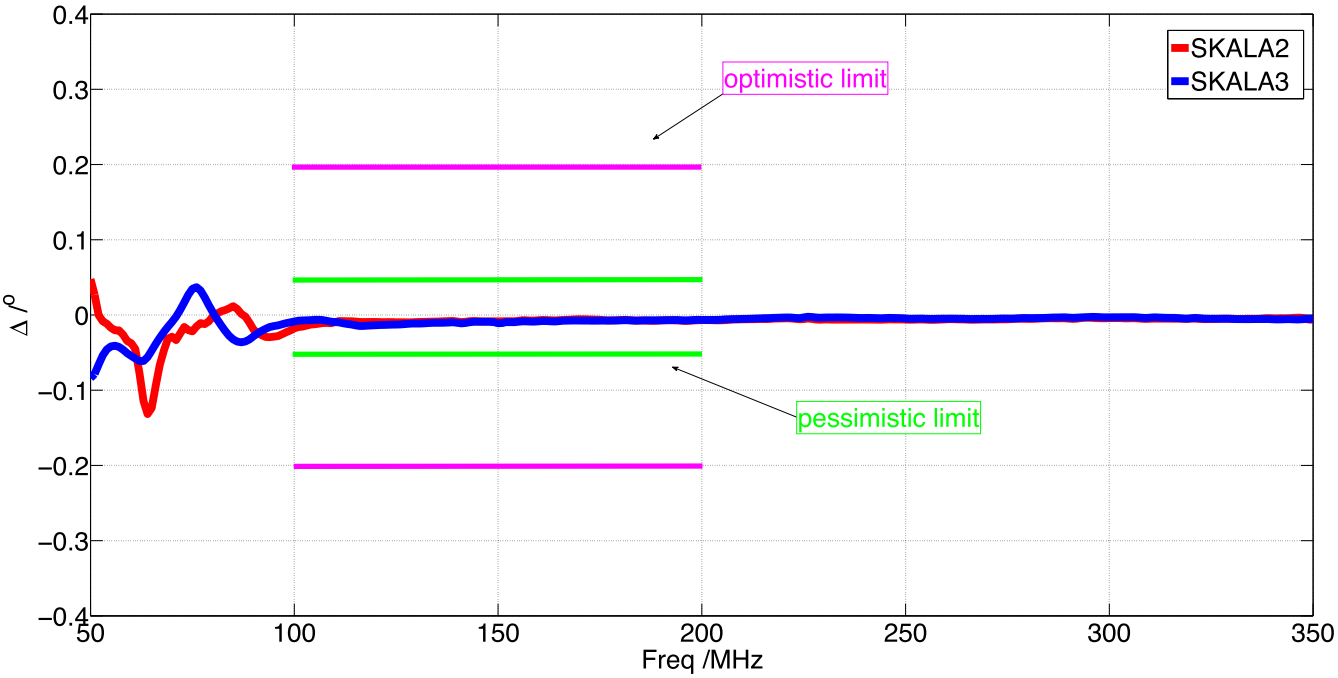

Figure 6. Phase gradient per fine channel for SKALA-2 and SKALA-3. The plot also shows the *optimistic* and *pessimistic* limits as defined in Trott & Wayth (2016).

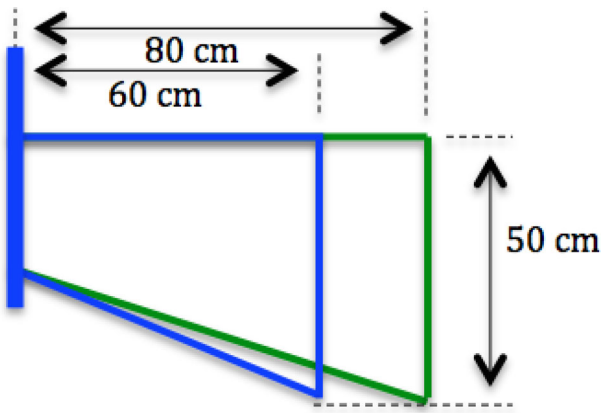

Figure 7. New lower antenna arm (green, SKALA-3) versus old arm (blue, SKALA-2).

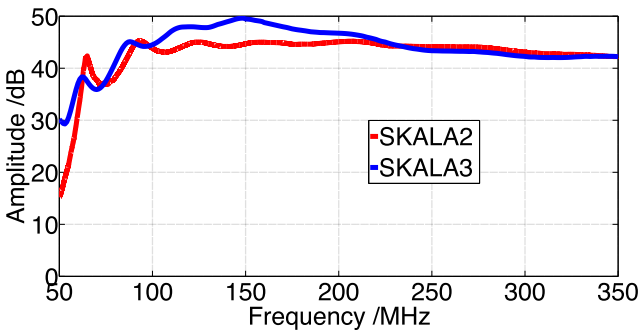

Figure 8. Amplitude of the LNA voltage passband when connected to SKALA-3 (blue) versus when connected to SKALA-2 (red). The plot shows the sharp feature found in the passband of SKALA-2 at 60 MHz.

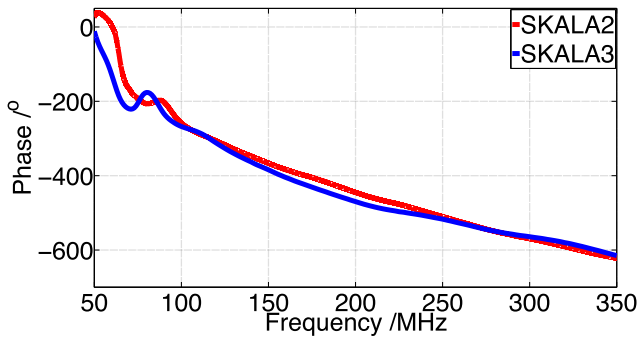

Figure 9. Phase of the LNA voltage passband when connected to SKALA-3 (blue) versus when connected to SKALA-2 (red).

figure starts to increase rapidly (18 pF gives in excess of 10 dB noise figure).

In order to bring the antenna impedance closer to the LNA input impedance, facilitating the match, we have enlarged the bottom dipole of the antenna (active at the lower end of the band). The design is shown in Fig. 7. This increases the footprint of the antenna to 1.6 × 1.6 m instead of 1.2 × 1.2 m. While it is possible from an electromagnetic point of view to interleave antenna footprints in a SKA station it may not be appropriate for maintenance of the antennas. We are exploring a larger station size (40 m) to support this new design while minimizing the impact in the station performance.

5.2 Improved antenna response and impact on SKA1-LOW sensitivity

With the changes presented above we recalculated the performance of the new version of the SKALA antenna (SKALA-3). Figs 8 and 9 show the new LNA amplitude and phase passbands when connected to the antenna impedance. Fig. 5 shows the amplitude residuals for SKALA-3, now within the requirements, for a third order polynomial fitted across three coarse channels. In Table 2 we

Table 2. Residuals obtained when fitting wider bandwidths.

Frequency (MHz)	δ(m = 5)	δ(m = 7)	δ(m = 9)
50	0.00073	0.00612	0.01327
100	0.00009	0.00017	0.00074
150	0.00090	0.00100	0.00110
200	0.00003	0.00003	0.00004

also list the residuals for wider bandwidths and a polynomial of order three fitting the data. We simulated for five coarse channels (3.75 MHz), seven coarse channels (5.25 MHz) and nine coarse channels (6.75 MHz). We observe an increase in the residuals when we try to fit a wider frequency bandwidth with a polynomial of order three but always staying below the required limit. Fig. 6 shows how the phase gradient has improved at all frequencies therefore still meeting the requirements in the EoR band. Finally, Fig. 10 shows the effect on the SKA1-LOW sensitivity when using the new antenna, SKALA-3. The sensitivity has been calculated using equation (1). This is also flatter across frequency. The antenna's directive gain (directivity) is one of the main contributors to the effective aperture and therefore to the sensitivity of the antenna as described in de Lera Acedo et al. (2015b). The change in the length of the bottom dipole of SKALA in order to improve the low frequency impedance match with the LNA has caused, as expected, a smoother transition between the bottom dipole and the second dipole. This has produced a flatter directivity of the antenna across frequency and therefore a flatter sensitivity pattern.

6 THE DELAY-SPECTRUM METRIC

A well-studied way to look at antenna spectral requirements is from the perspective of foreground *avoidance* in power spectrum space. In the avoidance scheme, smooth-spectrum foregrounds should, in the ideal case, occupy a wedge–shaped region of the two–dimensional power spectrum space (where the wavenumber k can be decomposed into $k_\perp$ and $k_\parallel$ that are the transverse and line-of-sight wave numbers, respectively) whereas the remaining area – the so-called EoR window – is dominated by the 21 cm emission (Datta, Bowman & Carilli 2010; Morales et al. 2012; Trott, Wayth & Tingay 2012; Vedantham, Udaya Shankar & Subrahmanyan 2012; Thyagarajan et al. 2013; Liu, Parsons & Trott 2014a,b). Sources have most of their emission at low $k_\parallel$ values although, due to the inherent chromatic interferometric response, this area increases with baseline length to resemble a characteristic wedge-like shape (Parsons et al. 2012; Trott et al. 2012; Vedantham et al. 2012; Liu et al. 2014a,b; Thyagarajan et al. 2015). In the most optimistic scenario, the EoR power spectrum can be directly measured in the EoR window, whose boundaries are set by the so-called *horizon limit*, i.e. the maximum delay that an astrophysical signal can experience, given by the separation of the two receiving elements. In practice, the boundaries of the EoR window can be narrowed by a number of mechanisms that spread power from the foreground dominated region into the EoR window, in particular calibration errors (Barry et al. 2016; Patil et al. 2016), leakage of foreground polarization (Bernardi et al. 2010; Jelić et al. 2010; Moore et al. 2013; Asad et al. 2015, 2016) and intrinsic chromaticity of the instrumental response. Recent attention has indeed been given to simulate and characterize the element response, particularly for the HERA (DeBoer et al. 2017), realizing that it may be one of the critical items responsible for spilling power from the wedge into the EoR window.

The HERA design leverages a highly-redundant array configuration that accumulates its maximum sensitivity on a limited number of $k_\perp$ modes, building on the results of the Precision Array to Probe the Epoch of Reionization (PAPER; Parsons et al. 2014; Jacobs et al. 2015; Ali et al. 2015). Like PAPER, HERA plans to employ a foreground avoidance scheme on a per-baseline base through the delay transform. In equation (5), $\widetilde{V}_b(\tau)$ is the delay (τ) transform (inverse Fourier transform) of the measured frequency visibility for a fixed baseline $V_b(\nu)$ (equation 6), that includes the sky brightness, $I(\widehat{s}, \nu)$ and the antenna's directional power pattern, $A(\widehat{s}, \nu)$. c is the speed of light, b is the baseline vector and $\widehat{s}$ is the direction

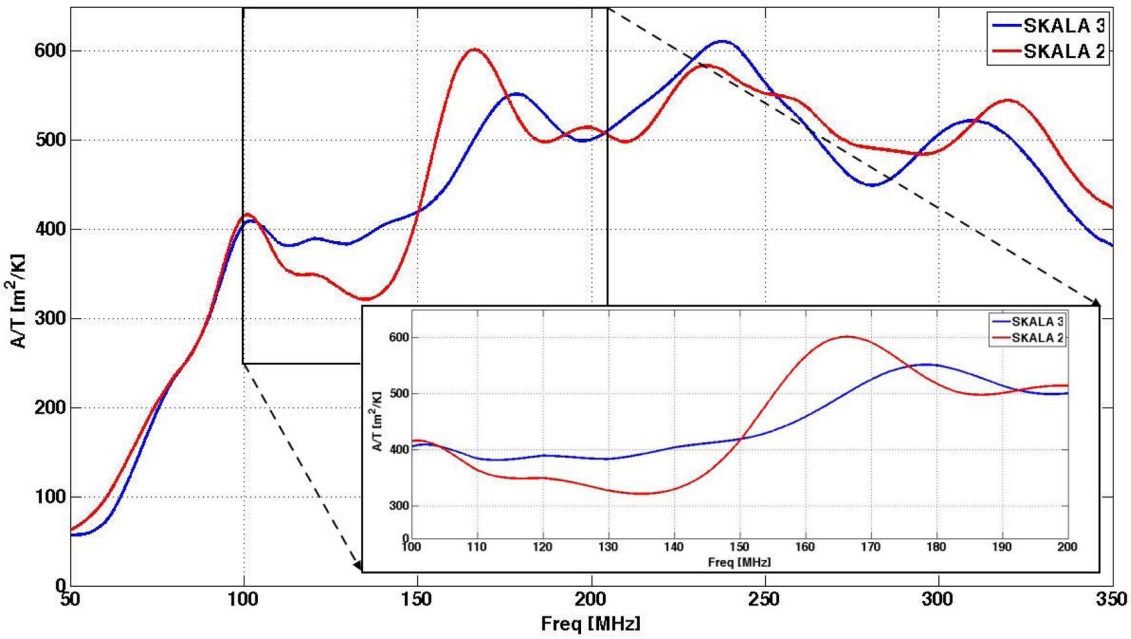

Figure 10. SKA1-LOW sensitivity at zenith with SKALA-2 and with SKALA-3 across the full band. Both calculations assume the same parameters (sky noise, station size, etc.) as described in de Lera Acedo et al. (2015b).

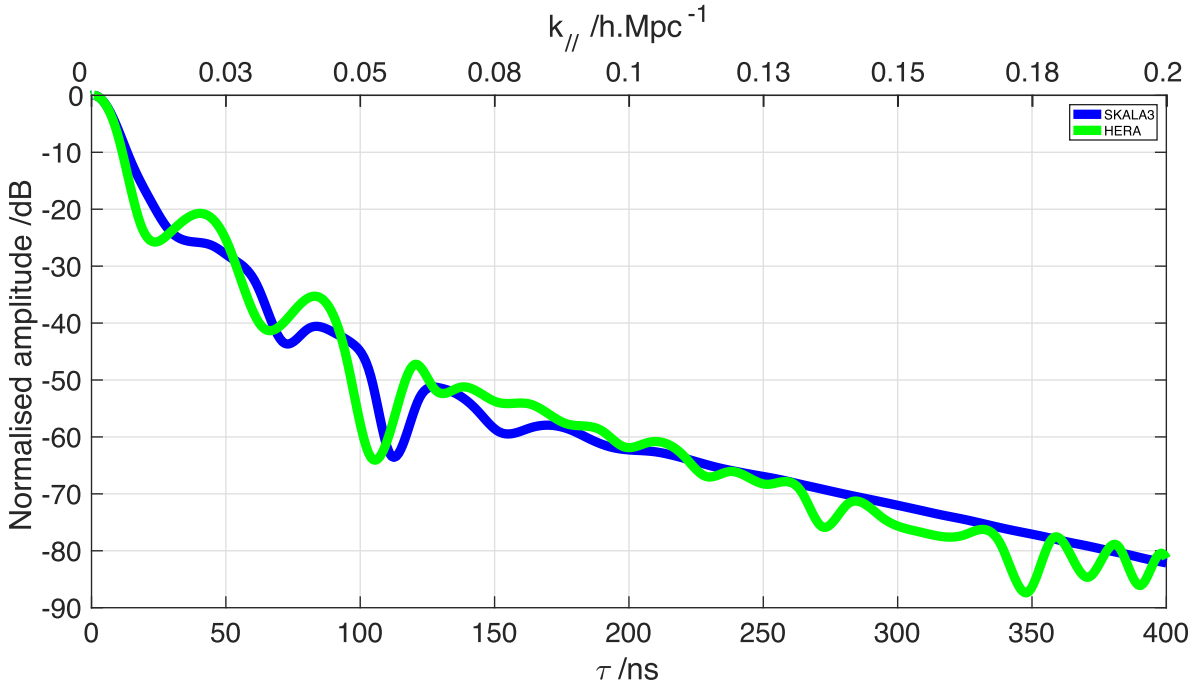

Figure 11. Comparison between the normalized voltage transfer function of the HERA antenna and SKALA-3 at zenith (including in both cases the effects of their matching to the LNA) in the band 100–200 MHz after applying a Blackman-Harris window (100–200 MHz) to both of them. This window is used to eliminate the noise caused by numerical artefacts in the calculation of the transfer function towards the edges of the band.

on the sky (unit vector). The sky power spectrum $P(k)$ can then be approximated by equation (7), where B is the effective bandwidth, Ω_b is the integrated beam response, k_B is the Boltzmann's constant and X and Y are cosmological parameters relating angular size and spectral frequency to cosmic volumes, respectively. For more details, see Parsons et al. (2012).

$$\widetilde{V}_b(\tau) \equiv \int V_b(\nu) \mathrm{e}^{\mathrm{i}2\pi\nu\tau} d\nu \tag{5}$$

$$V_b(\nu) = \int_{\mathrm{sky}} A(\hat{s}, \nu) I(\hat{s}, \nu) \mathrm{e}^{-\mathrm{i}2\pi\nu \frac{b\cdot\hat{s}}{c}} \tag{6}$$

$$P(\mathrm{k}) \approx \frac{X^2 Y}{4k_B^2} \left[\frac{\widetilde{V}_b^2(\tau)}{\Omega_b B/\lambda^4} \right] \tag{7}$$

The delay transform has therefore been used as a metric to characterize the response of the HERA dish (Ewall-Wice et al. 2016; Neben et al. 2016; Thyagarajan et al. 2016; Fagnoni & de Lera Acedo 2016).

Given its very compact configuration, HERA achieves its highest sensitivity on a 14.6 m baseline and, in order to suppress foregrounds to below the EoR level at the corresponding k mode, requires high suppression at high delays (DeBoer et al. 2017). Ewall-Wice et al. (2016) and Thyagarajan et al. (2016) show that the current dish+feed response suppresses foregrounds below the EoR signal at ∼300 ns; access to smaller k modes, however, can still be achieved using an optimal weighting scheme (Liu & Tegmark 2011; Ali et al. 2015). Although the SKA will adopt a different array configuration, motivated by imaging requirements that need a more random uv coverage, the delay-spectrum metric can be used to characterize its antenna response too.

Ewall-Wice et al. (2016) describes how to perform a simulated analysis of the antenna system to measure its capabilities for EoR detection using the delay-spectrum technique. We have followed a similar approach here but extended to include the effects of the matching to the LNA. The design goal is to reduce the response of the antenna in the delay spectrum for large values of delay (corresponding to large values of $k_\parallel$) to avoid contamination of the EoR window. The core EoR detection will be done using $k_\parallel$ modes greater than 0.1 h Mpc^{-1} and therefore we should make sure that any power introduced by reflections in our instrument is below the EoR H I signal. A plane wave incoming from zenith is used to excite the HERA antenna. The same process is used to excite the SKALA-3 antenna. Circuit models of the LNAs for both HERA and SKA have been connected to the antennas in the simulation to represent the effects of the mismatch between the antenna and the LNA in their response. Separate time domain full electromagnetic simulations (using the CST program) were then performed to obtain the output signal of the pair antenna+LNA for both systems. The transfer function of the antenna is then calculated by dividing in Fourier space the output voltage signal by the input signal (the plane wave) used as excitation. Finally, the calculated transfer function is transformed to the delay domain by applying an inverse Fourier transform. Figs 11 and 12 show this transfer function for both antennas in two frequency bands relevant to the CD/EoR science, 100–200 MHz and the extended band 50–250 MHz. These plots are normalized to the amplitude of the first incidence of the plane wave in the HERA feed after an initial reflection in the dish and to the direct incidence in the SKALA-3 antenna, respectively. These incidence times are used as $\tau = 0$ ns.

In Fig. 11 we can see that the SKALA-3 performance is comparable to that of the HERA antenna including feed and dish for a large portion of significant delays for the band 100–200 MHz. In Fig. 12 we can see how the response of SKALA-3 also seems to be competitive in the extended band (50–250 MHz). In these simulations the effects of the multiple reflections on the HERA dish are included. This result is likely to change when the effects of mutual coupling are included for both systems. In the case of SKA1-LOW, the antennas in a station will be arranged in a pseudo-random

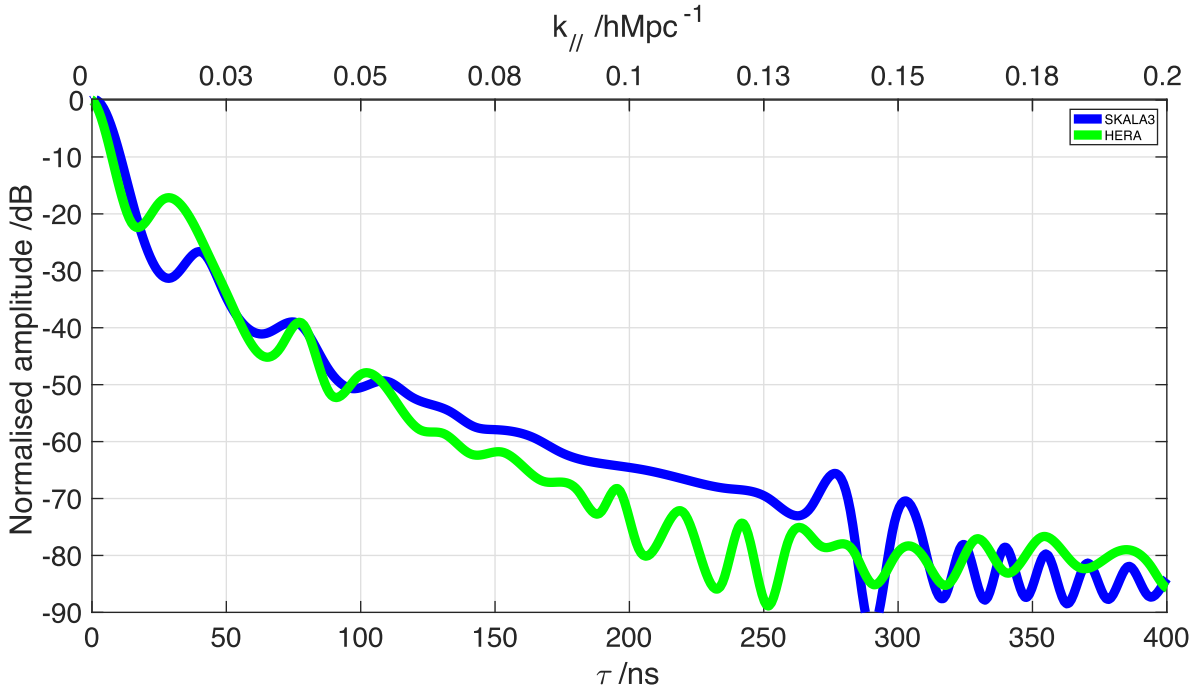

Figure 12. Comparison between the normalized voltage transfer function of the HERA antenna and SKALA-3 at zenith (including in both cases the effects of their matching to the LNA) in the band 50–250 MHz after applying a Blackman-Harris window (50–250 MHz) to both of them. This window is used to eliminate the noise caused by numerical artefacts in the calculation of the transfer function towards the edges of the band.

configuration and they will be placed at about 2 m from each other on average. However for HERA, the configuration is triangular-regular and the distance between antennas is 14.6 m. While the level of the coupling will be therefore higher for SKA, it is also worth noticing that the effects of mutual coupling tend to average out in random arrays (de Lera Acedo et al. 2011). The actual impact of coupling could therefore be assumed to be non-dominant, but further work will explore these effects in more detail. The HERA results shown here are consistent with those shown in Ewall-Wice et al. (2016), although the results in this paper include the effects of the mismatch with the actual LNA.

It is also worth noting that HERA only uses relatively short baselines to prevent the contamination of the EoR window.

7 CONCLUSIONS AND FUTURE WORK

In this paper we have presented two different analyses of the passband response of realistic antennas for 21 cm cosmology experiments. One is based on fitting a local low-order polynomial to the passband in order to model and calibrate it. The second is based on building an antenna design free of spectral structure at the relevant scales for the detection of the EoR following the delay-spectrum technique proposed for HERA. The analyses have been done using the improved log-periodic antenna proposed for SKA1-LOW (SKALA-3).

Using electromagnetic and redio frequency (RF) computer simulations of the antennas and LNAs, we have shown that with minor modifications on the antenna and LNA design it is possible to improve the impedance matching that dominates the spectral performance of the system meeting the passband smoothness requirements established in Trott & Wayth (2016). Furthermore, these modifications result in a design able to use the delay-spectrum technique provided that other considerations are also taken into account (e.g. the effects of mutual coupling and side lobes have not been taken into account in this analysis). The main parameters of the antenna such as sensitivity are only slightly affected by these changes, however, the overall response has been flattened at reduced spectral scales over the frequency range.

These analyses are now going to be validated using measurements on a prototype. Furthermore, we will shortly add to the study an analysis of the effects of mutual coupling and other sources of spectral features in the instrument's passband (e.g. side lobes as in Thyagarajan et al. 2016). In particular, beam-formed arrays of antennas are studied in paper II in this series (Trott et al. 2017). In Trott et al. (2017) realistic interferometric and sky simulations (including frequency-dependent primary beam shapes and array configuration) are used to study the calibration performance of the antennas. It applies a weighted least squares polynomial estimator to assess the precision with which each antenna type can calibrate the instrument, and compares to the tolerances described in Trott & Wayth (2016). Further work will also be done to assess the impact of the spectral smoothness of realistic beam-forming technologies and techniques.

ACKNOWLEDGEMENTS

The authors thank Paul Alexander and the SKA Office for useful discussions. The authors would like to acknowledge their SKA Aperture Array Design Consortium colleagues for their help and discussions on the topic. This research was supported by the Science & Technology Facilities Council (UK) grant: *SKA, ST/M001393/1* and the University of Cambridge, UK. This research was also supported under the Australian Research Council's Discovery Early Career Researcher funding scheme (project number DE140100316), and the Centre for All-sky Astrophysics (an Australian Research Council Centre of Excellence funded by grant CE110001020).

This work was supported by resources provided by the Pawsey Supercomputing Centre with funding from the Australian Government and the Government of Western Australia. We acknowledge the iVEC Petabyte Data Store, the Initiative in Innovative Computing and the CUDA Center for Excellence sponsored by NVIDIA at Harvard University, and the International Centre for Radio Astronomy Research (ICRAR), a Joint Venture of Curtin University and The University of Western Australia, funded by the Western Australian State government. The authors also acknowledge support from the Royal Society and the Newton Fund under grant NA150184. This work is based on the research supported in part by the National Research Foundation of South Africa (Grant Number 103424).

REFERENCES

Ali Z. S. et al., 2015, ApJ, 809, 61
Asad K. M. B. et al., 2015, MNRAS, 451, 3709
Asad K. M. B. et al., 2016, MNRAS, 462, 4482
Barry N., Hazelton B., Sullivan I., Morales M. F., Pober J. C., 2016, MNRAS, 461, 3135
Bernardi G. et al., 2010, A&A, 522, A67
Datta A., Bowman J. D., Carilli C. L., 2010, ApJ, 724, 526
de Lera Acedo E., Razavi-Ghods N., Ovejero D. G., Sarkis R., Craeye C., 2011, ICEAA (International Conference on Electromagnetics for Advanced Applications). IEEE, Turin, p. 390
de Lera Acedo E., Drought N., Wakley B., Faulkner A., 2015a, ICEAA (International Conference on Electromagnetics for Advanced Applications). IEEE, Turin, p. 839
de Lera Acedo E., Razavi-Ghods N., Troop N., Drought N., Faulkner A. J., 2015b, Exp. Astron., 39, 567
DeBoer D. R. et al., 2017, PASP, 129, 045001
El-makadema A., Rashid L. K. Brown A., 2014, IEEE Trans. Antennas Propag., 62, 1673
Ewall-Wice A. et al., 2016, ApJ, 831, 196
Fagnoni N., de Lera Acedo E., 2016, ICEAA (International Conference on Electromagnetics for Advanced Applications). IEEE, Cairns, Australia, p. 629
Gonzalez-Ovejero D., de Lera Acedo E., Razavi-Ghods N., Craeye C., Garcia Munoz L. E., 2011, in Antennas and Propagation Symposium. IEEE, Spokane, Washington, p. 1762
Jacobs D. C. et al., 2015, ApJ, 801, 51
Jelić V., Zaroubi S., Labropoulos P., Bernardi G., de Bruyn A. G., Koopmans L. V. E., 2010, MNRAS, 409, 1647
Koopmans L. et al., 2015, Proc. Sci., The Cosmic Dawn and Epoch of Reionisation with SKA, SISSA, Trieste, PoS#1
Liu A., Tegmark M., 2011, Phys. Rev. D, 83, 103006
Liu A., Parsons A. R., Trott C. M., 2014a, Phys. Rev. D, 90, 023018
Liu A., Parsons A. R., Trott C. M., 2014b, Phys. Rev. D, 90, 023019
Mellema G. et al., 2013, Exp. Astron, 36, 235
Moore D. F., Aguirre J. E., Parsons A. R., Jacobs D. C., Pober J. C., 2013, ApJ, 769, 154
Morales M. F., Hazelton B., Sullivan I., Beardsley A., 2012, ApJ, 752, 137
Neben A. R. et al., 2016, ApJ, 826, 199
Parsons A. R., Pober J. C., Aguirre J. E., Carilli C. L., Jacobs D. C., Moore D. F., 2012, ApJ, 756, 165
Parsons A. R. et al., 2014, ApJ, 788, 106
Patil A. H. et al., 2016, MNRAS, 463, 4317
Pozar D., 2011, Microwave Engineering, 4th edn. Wiley, New York
Razavi-Ghods N., de Lera Acedo E., El-Makadema A., Alexander P., Brown A., 2012, Exp. Astron, 33, 141
Thyagarajan N. et al., 2013, ApJ, 776, 6
Thyagarajan N. et al., 2015, ApJ, 804, 14
Thyagarajan N., Parsons A., DeBoer D., Bowman J., Ewall-Wice A., Neben A., Patra N., 2016, ApJ, 825, 9
Tingay S. J. et al., 2013. , PASA, 30, 7
Trott C. M., Wayth R. B., 2016, PASA, 33, e019
Trott C. M., Wayth R. B., Tingay S. J., 2012, ApJ, 757, 101
Trott C. M., de Lera Acedo E., Wayth R. B., Fagnoni N., Sutinjo A. T., Wakley B., Punzalan C. I., 2017, MNRAS, in press, Paper II
Turner W., 2015, SKA-TEL-SKO-0000008, SKA Phase 1 System Level 1 Requirements (Rev 6)
Vedantham H., Udaya Shankar N., Subrahmanyan R., 2012, ApJ, 745, 176

This paper has been typeset from a TEX/LATEX file prepared by the author.